OpenFOAM® Journal

Volume 4 [Full Papers], Pages 26–40
ISSN: 2753-8168

Comparison of CFD-DEM and MP-PIC in the Simulation of Metal Powder Conveying for Laser Metal Deposition

Lorenzo Pedrolli[1,*], Beatriz Achiaga[1], Inger Martínez de Arenaza[2], and Alejandro Lopez[1,*]

[1]Faculty of Engineering, University of Deusto, Bilbao (ES)

[2]Department of Mining and Metallurgical Engineering and Material Science, University of the Basque Country (EHU/UPV), Bilbao (ES)
Email address: l.pedrolli@deusto.es
Email address: alejandro.lopez@deusto.es

DOI: https://doi.org/10.51560/ofj.v4.91
Results with version(s): OpenFOAM® v9
Repository: https://github.com/DeustoFoam/LagrangianComparisonOFW17

Abstract. Pneumatic conveying of fine powders is essential for many industrial processes, including Laser Metal Deposition (LMD), a Direct Metal Additive Manufacturing (DMAM) technology that builds solid objects layer-by-layer using a laser to melt metal powder. To optimize the process, it is necessary to have a correct understanding of the powder's behaviour under the process condition.

The coupled Computational Fluid Dynamics - Discrete Element Modelling (CFD-DEM) and MultiPhase - Particle In Cell (MP-PIC) are two popular Eulerian-Lagrangian models to simulate particle laden flows. This study compares them to analyse powder behaviour in a small channel of LMD machines. Results from the two methods differ significantly, with CFD-DEM offering a more accurate representation of the physical reality, while MP-PIC is more computationally efficient. The study finds that the CFD-DEM method produces higher fluctuations in the solids flow rate due to the formation of particle clusters, while MP-PIC displays a smooth and essentially uniform flow. The results suggest that CFD-DEM should be used for more accurate and detailed studies of solids flow rate in pneumatic conveying systems, while MP-PIC can be used for preliminary studies and design optimization.

1. Introduction

In industrial processes it is very common to use materials in form of fine powders. In Laser Metal Deposition (LMD), a Direct Metal Additive Manufacturing (DMAM) technology, the desired solid object is built by the layered deposition of metal in powder form molten by a laser. An accurate powder delivery during the layer deposition is crucial for the manufacturing process. Observing manufactured parts from the work of Dadbakhsh [1], and their roughness profile, we can assess the presence of hills and valleys in the tool head's direction of travel. Periodic flow phenomena are detectable at the nozzle exit, and flow variation has been observed to have a measurable effect on the deposition quality [2].

Pneumatic powder feeders are the most popular for the feedstock handling in LMD systems. The powder is gradually fed to the pneumatic conveying system using metering equipment, which provide a uniform gas/powder mixture flow. Reaching the nozzle, several different configurations are possible: off-axis, discrete coaxial, continuous coaxial, annular continuous and discrete laser beam [3]. This study aims to find a base to describe the last part of the pneumatic conveying system, inside the nozzle conducts, as represented by Fig.1.

The periodic variation over time of the powder fed to the process is certainly not the only factor influencing part's quality, however it might have a measurable effect. Previous studies on LMD equipment consider time-averaged powder flows [4] [5], whereas the variability of the mass flow rate in pneumatic conveying systems is a known and documented phenomenon [6] [7] [8] [9]. The pneumatic conveying flow is influenced by a number of factors, which are abundantly discussed in literature [10] [11] [12], and are

* Corresponding author

Received: 31 August 2022, Accepted: 27 December 2023, Published: 9 February 2024

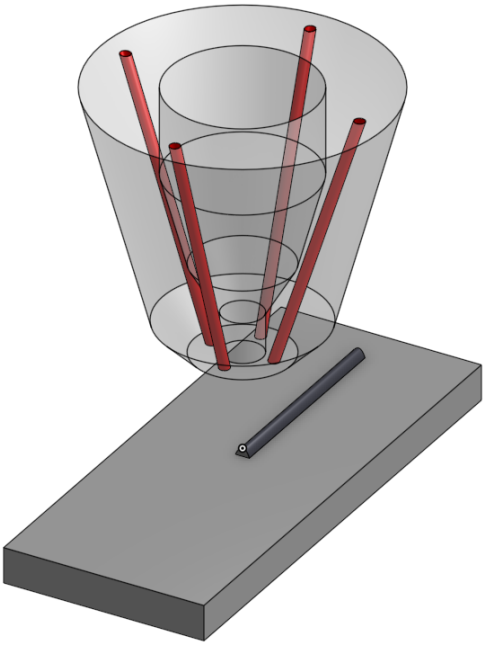

Figure 1. Example draft of a typical discrete LMD nozzle with four converging powder conveying channels (highlighted in red), and a central hole for the laser to shine through and for the shielding gas.

still under active investigation due to the great variability in the characteristics of powders and the levels of detail needed by each application.

Variations in the pneumatic conveying flow can be self-induced and regular. This variation in particle velocity and instantaneous powder mass flow rate directly affects the material deposition rate of the LMD process. Zhou et.al [13] present a study for a bigger scale pneumatic conveying system, where pulsating flow phenomena and periodic flow regimes can be observed in a pipe with a flat rectangular section, both in the experiments and the simulation. The flow oscillations seem to be self-excited. In the CFD-DEM dilute phase simulation of a horizontal channel by Zhao [14], where the Lagrangian phase is not influencing the continuous phase, 1-way coupling, display a uniform particle motion and velocity driven by the viscous effects. However, taking that influence into account, the fluid flow displays periodic bands of particle concentration in the flow direction. Pulsations in the mass flow rate of pneumatic conveying systems has been measured experimentally, Alkassar et.al. [15] experimentally analyzed a pneumatic conveying pipeline with dilute flow and dune flow. The study showed regular pulsations in the pressure along different position on the pipe, with wavelet analysis showing a dependence of the pulsations on the solid loading and characteristics.

The use of numerical models in pneumatic conveying has increased with computational technology. Continuum-based models, such as the Two-Fluid Model (TFM), are widely used, but their effective use depends on constitutive relations and developing a TFM model that can reproduce all flow regimes and transitions remains a challenge. TFM studies focus on powders or fine particles, but mixtures of particles require increased detail and adherence to experiments, which can be achieved using Lagrangian models [16], which may be further classified by the type of coupling between particles and fluid:

One-way coupling: If the volumetric concentration of particles is low enough, the influence that the particles exert on the fluid phase may be neglected.

Two-way coupling: In this case the force exerted by the particles on the fluid is no longer neglected.

Four-way coupling: In this case also particle-particle interactions are taken into account.

Existing literature on LMD nozzle systems which employs a Lagrangian model for the powder phase, mostly analyzes the process using MP-PIC [17] [4] or Discrete particle Models 1-way or 2-way coupling [17], motivated by the low particle loading in the system. Previous studies report how the particle-particle interaction in CFD-DEM simulations leads to the formation of clusters [6] [18], and therefore powder mass flow rate fluctuations. Even though the MP-PIC model find most of its applications in large reactor models, it is used in the modelling of pneumatic conveying of solids [19].

The present work aims to compare ways of simulating their presence and emergence in the pipelines within the Laser Metal Deposition (LMD) equipment, especially in the final length of thin tubing inside

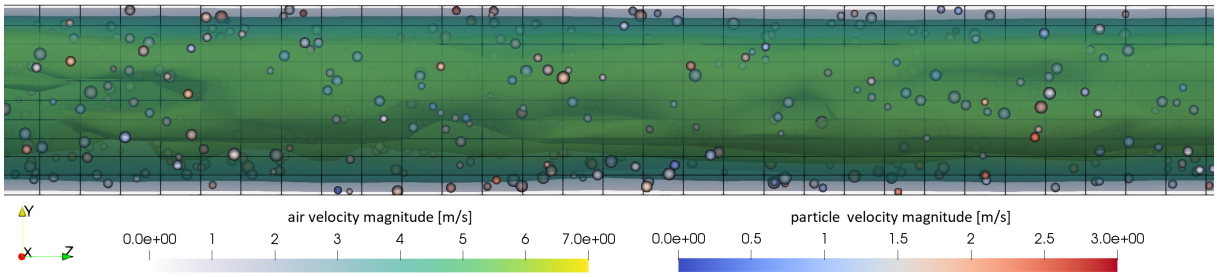

Figure 2. Lateral view of the simulation domain with velocity magnitude contours. The complete domain is a simple, straight pipe. The image highlights the spatial distribution of particles in the diameter.

the nozzle. Using OpenFOAM's `denseParticleFoam` library [20], the objective is to compare a fully coupled, unresolved CFD-DEM simulation with a less computationally expensive MP-PIC one [21] [22], even though the latter requires more empirical parameters [23]. If the two methods are both compatible with the phenomenon, their results should agree to a certain measure, otherwise one has to be preferred over the other. Unresolved CFD-DEM solves the physical interactions between particles and between each particle and fluid, in this case completing the picture to 4-way coupling, and for this reason it is expected to be the one which gives the most physically accurate results, whereas MP-PIC should capture more averaged behaviors.

Given the lack of experimental data, it is important to acknowledge the limitations of the present study. The numerical models and assumptions made in this work aim to capture the behavior of the powder flow in a simplified scenario, but may not fully reflect the complexity of the real system. It is possible that other factors not considered in this study, such as particle shape or interparticle forces, could affect the accuracy of the results. Therefore, further experimental validation would be necessary to confirm the conclusions drawn from this work. Nonetheless, the present study provides valuable insights into the behavior of powders in a laminar flow and the relative performance of different Lagrangian models in simulating such systems.

2. Conveying pipe configuration

2.1. **Simulation domain.** LMD deposition nozzles can present in different designs, with different applications. This work is conducive to the analysis of more complex cases. Of particular interest are discrete nozzles and continuous nozzles with internal channels. An example draft of such a nozzle is represented in Fig. 1, where the four converging channels are highlighted.

The considered geometry is a straight pipe with circular cross-section, placed horizontally. The inlet is on the origin, and the pipe is oriented along the positive Z axis in the reference frame XYZ, the flow is introduced in the positive Z direction. For this comparison, gravity has the value of $\mathbf{g} = [0, -9.81, 0]$ m/s^2, therefore acting in the radial direction negative Y. Typical LMD applications see the pipe close to vertical; this can be obtained simply by changing the vector component values in the appropriate case file, but a horizontal configuration simplifies the representation.

The pipe has a diameter of $D = 1.25$ mm and a length of $L = 300$ mm, resulting in an L/D ratio of 240, higher than Li et al.'s work on simulating powder stream characteristics in a laser metal deposition nozzle using a 3D model [17]. In this case, the length was chosen to ensure the full development of the flow conditions, as highlighted in Section 3.1. Since the OpenFOAM code is written for unresolved simulations, the pipe was discretized with a mesh with cell volume larger than the maximum particle size. Convergence of the fluid flow was verified for a mesh with 33600 elements, as shown in Fig. 3.

The imposed inlet velocity set is in Tab. 1, the comparison is for the values $U_{g,A} = 10$ m/s and $U_{g,B} = 5$ m/s. The corresponding flowrates $\dot{V}_g$ are calculated for the 1.25 mm diameter pipe. As found in [4], the particles will be introduced with the same velocity as the gas, from the inlet plane, with the injection rate $\dot{Q}_p$ specified in particles per second. Considering the distribution shown in Fig. 4, the expected mass flow rate of the powder is calculated and reported in the table as $\dot{m}_p$. The pipe length was chosen to allow the transition from the virtual inlet conditions (both for particles and gas) to the established flow [24]. In both cases the theoretical volumetric solid fraction being transported is $\alpha_s = \dot{m}_s / \left(\rho_s \dot{V}_g\right) = 0.004$, which is well within the dilute flow particle loading [25].

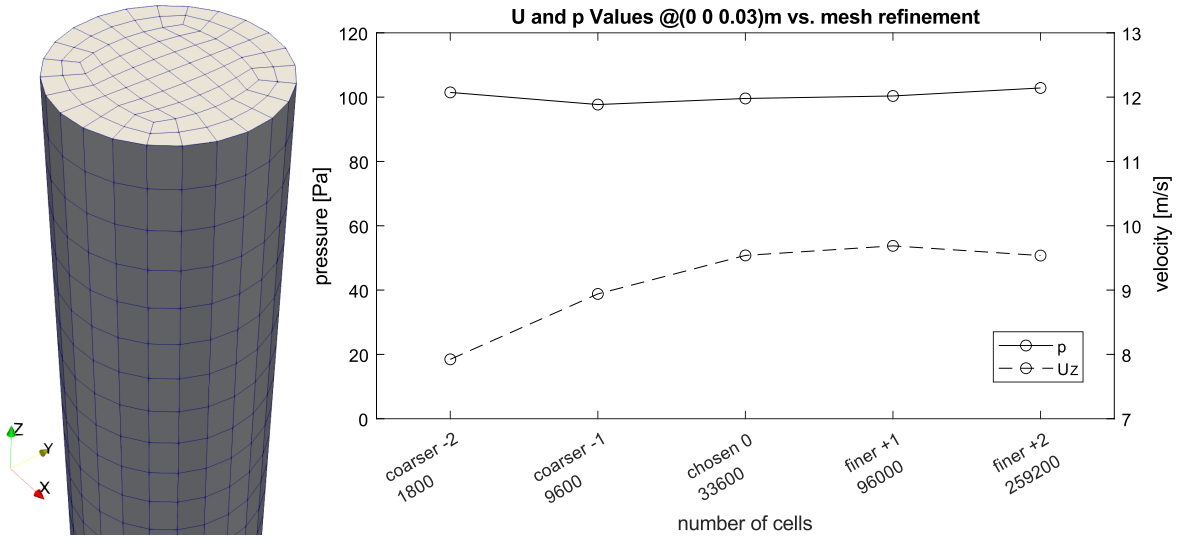

Figure 3. End view of the pipe, with detail on the chosen mesh. Convergence analysis of the fluid flow, verified for a mesh with 33600 elements, on the pressure p and the axial velocity U_Z.

In this discussion, the flow is modeled with four-way coupling to account for both particle-fluid and particle-particle interactions. This modeling approach is crucial because it considers the forces exerted by particles on the fluid, as well as the reaction of the particles to these forces. Neglecting these forces would result in an incomplete representation of the physical phenomena within the system.

The `coneInjection` model, employing a disk injector, might be utilized to generate particle flow. However, it lacks a mechanism to detect particle overlap within the disk, a phenomenon that occurs randomly, particularly at high parcel flow rates and low velocities. It is advisable to incorporate an overlap check functionality into the injection model. The occurrence of initial particle overlaps results in the creation of stray particles with high transversal velocities, which can introduce uncontrolled disturbances in the pipe. Another adverse consequence is the potential spike in the local Courant number, rendering the simulation more unstable. It is recommended to mitigate this issue.

To circumvent these issues, particles are introduced into the system using the `coneInjection` model in the point injector configuration. A hexagonal pattern composed of 99 points is uniformly distributed on a disk located 1 mm ahead of the inlet patch. The diameter of the disk is 1 mm, slightly smaller than the pipe diameter, to prevent initial overlaps between particles and the wall boundary. Particles are injected with a uniform velocity and a randomized start of injection, resulting in a continuous stream of particles. The diameter of the particles is randomly chosen to align with the size distribution model.

Table 1. Injection rates for gas $[\cdot]_g$ and particles $[\cdot]_p$

Parameter	Case A	Case B	Unit
U_g	10	5	m/s
$\dot{V}_g$	0.74	0.37	l/min
$\dot{Q}_p$	300×10^3	150×10^3	particles/s
$\dot{m}_p$	0.399	0.198	g/s

2.2. **Models and parameters.** A common shielding gas used in Directed Energy Deposition (DED) is Argon, the considered fluid properties are resumed in Tab. 2 for the standard conditions of $T = 25°C$ and $p = 1$ atm. Kussin and Sommerfeld [26] observed that the gas-solids interaction does not cause turbulence phenomena, with a significant decrease in turbulent intensity for a range of particle sizes which contains the ones considered in this study. Given the chosen flow velocities, shown in Tab. 1, the Reynolds number is $Re < 1000$ for both cases, justifying the assumption of laminar flow.

The material under investigation is AISI 316L austenitic stainless steel gas-atomized powder (MetcoAdd^{TM} 316L), which is fully dense and spherical in shape. The sample was provided by a source which is currently using LMD equipment, and its manufacturer (Oerlikon metco) declares it to be suitable for DED processes. The Particle Size Distribution (PSD) is represented by a Rosin-Rammler model and depicted

Table 2. Carrier gas properties, Argon.

Parameter	Value	Unit
ρ_g	1.6355	kg/m^3
μ_g	2.2624×10^{-5}	$Pa \cdot s$
ν_g	1.385×10^{-5}	m^2/s

in Fig. 4. The median diameter of the powder is $d_{50} = 66.9$ μm, with minimum and maximum cutoffs of 40 μm and 110 μm, respectively. The dictionary parameters used in the analysis are experimentally determined by fitting the PSD of a powder sample, as shown in Fig. 5.

The powder properties were measured by Nan et.al. [27] and reported in Tab. 3. The coefficient of restitution $e = 0.9$ indicates a relatively elastic collision between hard steel and glass, suggesting a significant conservation of kinetic energy, minimal deformation and energy dissipation. This implies a rigid interaction between the materials. This value applied for the MP-PIC cloud is used to determine the empirical constant `alpha` related to the damping coefficient for the DEM cloud, according to the heuristic relation provided by Tsuji et.al. [28]. The friction coefficient μ is inferred from a DEM simulation to match the experimental results in that specific application in the article by Nan et al. [27].

OpenFOAM implements the MP-PIC (Multi-Phase Particle-In-Cell) model [29]. The MP-PIC method treats a certain number of particles with the same physical properties as a parcel and calculates particle collisions through solid-phase normal stress model. The explicit three-dimensional packing model used in this work is described by Snider [21], and the particle stress is determined by using the implemented Harris-Crighton model [30]. The latter relies on the knowledge of the void fraction, therefore it is not suitable for fine meshes of the Eulerian phase for which cells might become fully occupied by a single parcel.

CFD-DEM calculates the motion of particles by following Newton's second law and quantifies the interactions between particles or between particle and wall by soft-sphere models: this work uses the spring-slider-dashpot (SSD) contact model available in OpenFOAM v9. It implements the no-slip model of Mindlin, which combined with the Hertzian theory of contact between spheres results in a non-linear spring model, to which dashpots are added in parallel to dissipate energy and account for the eventual hysteresis of the materials [10]. The tangential forces are modeled using a dashpot in parallel to a linear spring [28]. The SSD contact model parameters are set according to the AISI 316L powder properties reported in Tab. 3. By adopting a soft-sphere approach rather than relying on hard spheres, one can accurately capture the intricate dynamics of particle interactions and material behavior. This becomes particularly significant when considering the eventual formation of dense clusters.

CFD-DEM coupled solvers can be classified as resolved or unresolved approaches. In resolved CFD-DEM coupled solvers, the fluid force acting on a particle can be calculated by integrating the pressure and velocity fields in its surface. This approach requires a dense grid to obtain accurate fluid flow in CFD, which limits its applicability to particle-laden flow with a higher number of particles. In contrast, the unresolved approach of the CFD-DEM coupled solvers uses an empirical drag model based on the relative velocity and volume fraction of the fluid flow. Particle tracking is updated using an averaging method in each cell, and a dense grid is not needed to obtain an accurate drag force [31].

The unresolved approach loses detailed information about individual particle behavior and interactions, limiting the accuracy in representing phenomena like particle clustering, complex particle motions, and inter-particle forces, especially for more complex particle shapes. Unresolved simulations rely on simplified empirical drag models, which may not fully capture the range of particle behaviors and flow conditions. The unresolved approach may not be suitable for studying fine-grained phenomena that require a detailed representation of particle interactions. Despite these limitations, the unresolved approach is valuable for studying bulk behavior, overall system dynamics, and macroscopic effects in large-scale particle-laden flows.

This work is focused on particle unresolved CFD-DEM simulation, as resolved simulations are generally avoided in the study of industrial equipment due to their impractical computational cost.

The external forces acting on both the MP-PIC parcels and DEM particles are compatible for this study. In both cases, each Lagrangian discrete phase element is described by the same PSD and has the same density, since in both cases each element describes a single particle. The drag model is the one described by Gidaspow [32], which combines the Ergun dense phase model for volumetric fluid fractions $\alpha_g < 0.8$, with the Wen-Yu disperse phase model. This is used and validated for spherical particles, for any particle concentration up to close packing.

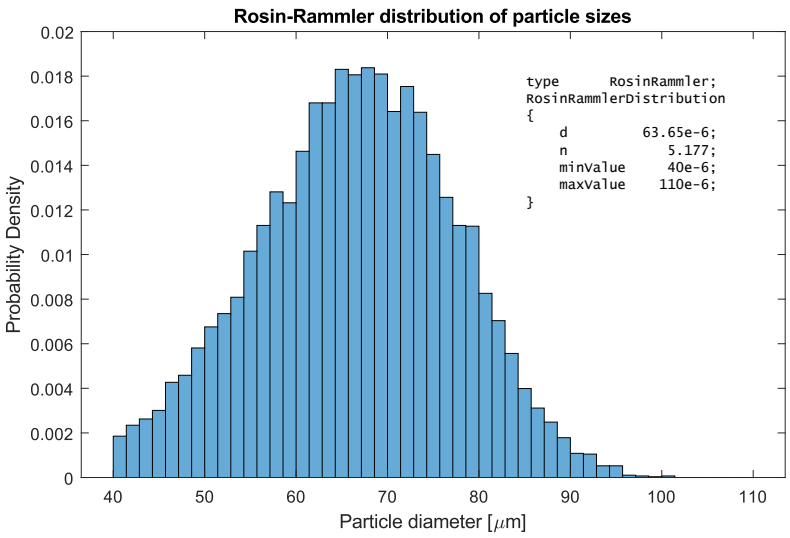

Figure 4. Probability density of the particle size. It is generated using the RosinRammler model implementation of OpenFOAM 9. The parameters d and n have been measured form the powder sample.

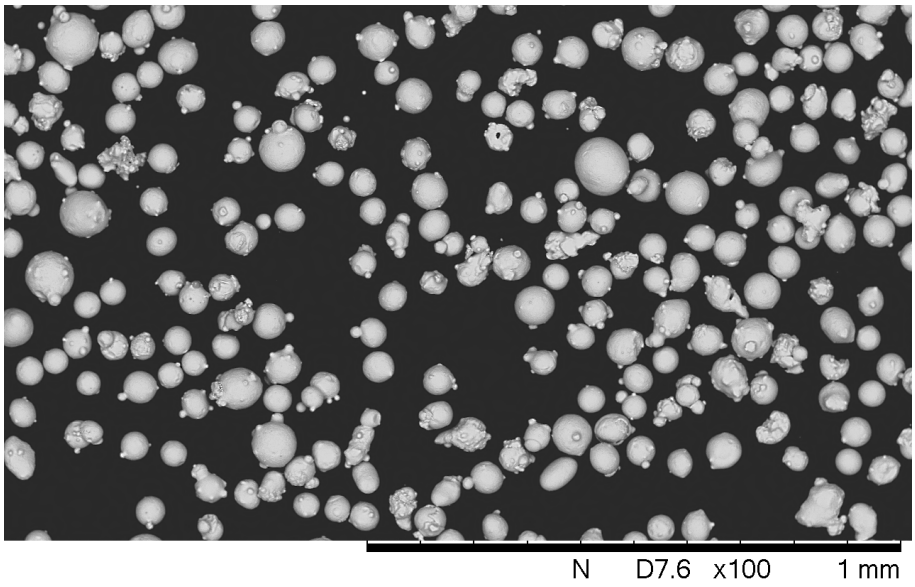

Figure 5. SEM image of a powder sample, used to determine the PSD.

Table 3. DEM particles properties for SS316L.

Parameter	Value	Unit
ρ_p	7980	$\mathrm{kg/m^3}$
ν_p	0.3	–
$E_{p,0}$	2.11×10^{11}	Pa
E_p	2.11×10^{7}	Pa
G_p	8.11×10^{6}	Pa
e	0.9	–
α	0.12	–
μ	0.52	–

An approximation of the critical time-step can be found in [10], considering the following equation:

$$\Delta t_c = \frac{\pi R_{min}}{v_R} = \frac{\pi R_{min}}{\lambda} \sqrt{\frac{\rho_p}{G_p}} \tag{1}$$

where v_R is the speed of Rayleigh waves, which is the mode that account for most of the energy transfer in powders (67%) along with distortional (26%) and dilational (7%) [10]. R_{min} is the minimum particle radius, ρ_p the density, ν_p is the Poisson's ratio of the metal particles. G_p is the particle's shear modulus, calculated from the Young modulus E_p as:

$$G_p = \frac{E_p}{2\ (1+\nu_p)}. \tag{2}$$

The Rayleigh wavelength can be approximated with the following:

$$\lambda = 0.8766 + 0.1631\nu_p \tag{3}$$

According to this formula, for a minimum diameter of 40 μm, with common values for 316L stainless steel from [27], would require $\Delta t_c = 2.13 \times 10^{-8}$ s. Such a small value would dilate the computation time by orders of magnitude.

In the context of DEM simulations for collision-dominated flows, reducing the Young's modulus to obtain a larger critical time-step is a common practice, since its impact on the results is limited [33]. Therefore, a reduced Young's modulus of $E_p = 2.11 \times 10^7$ Pa has been adopted in our simulations, which implies a critical time-step of $\Delta t_c = 2.13 \times 10^{-6}$ s. However, when effects such as dense phase and cohesion are present, certain parameters may need to be scaled accordingly [34]. In this case, the scaling would be necessary only for the parameter α, related to the damping coefficient of the spring-slider-dashpot model of the DEM case, calculated using according to the work by Tsiji et.al. [28]. Increasing the order of magnitude of the elastic modulus to approach the measured one, adjusting the time-step and α accordingly and setting a shorter simulation time, did not affect the general particle's behavior.

Furthermore, in addition to the dynamic effect of the contact, the particle relative velocities should also be considered when calculating the time-step. In the Rayleigh critical time-step, the particles may travel a significant distance compared to their size. For instance, for a characteristic speed of $V_c = 10$ m/s and $\Delta t_c = 4.76 \times 10^{-6}$ s, a particle would move 47.6×10^{-6} m.

In OpenFOAM, a separation margin between particles is used to approximate the contact. For the `collidingParcel` type, a maximum distance $\Delta\delta_{max}$ between centroids can be specified with `maxInteractionDistance`, below which a collision is assumed to be taking place. This maximum distance can be set equal to the maximum particles' diameter. At this point, the particles enter within interaction range, and the solver checks their reciprocal positions and velocities. To avoid skipping to the other side of the interaction or obtaining excessive overlap, the sub-step advancements must be small enough. The time-step is divided into a defined number of sub-steps defined by `collisionResolutionSteps`, increasing the time resolution for each contact and allowing the simulation to use of a time-step Δt that is a multiple of Δt_c. Another Courant number can be defined based on the relative velocity of the particles, the maximum interaction distance, and the global or base time-step. This Courant number ensures that the particles will enter within the sphere of influence without skipping:

$$Co^{DEM} = \frac{U_p\ \Delta t}{\Delta\delta_{max}} \tag{4}$$

where U_p is the individual particle's velocity.

2.3. **Solution schemes.** To aid with the comparison, solver settings were kept consistent between the two simulations. Separate steady-state simulations were used to initialize the Eulerian phase flow, which was then transferred to the transient case with `mapFields`.

The `cloudProperties` dictionary was used to define a `cellPoint` interpolation for both the velocity `U.air` and phase concentration `alpha.air` for Eulerian field values interpolation to the Lagrangian phase, as it demonstrated improved stability over `cell` interpolation. A semi-implicit Eulerian integration scheme was employed for the Lagrangian phase.

To solve the pressure field, `smoothSolver` with a `GaussSeidel` smoother was used, as it was observed to be more stable than `GAMG`. The latter sometimes caused pressure instability, leading to simulation crashes. However, the filtered pressure values were found to be similar in both cases. `GAMG` with a `GaussSeidel` smoother was used to solve the `alpha` field, while for the velocity field `U.air`, better residual stability was obtained using `PBiCGStab` with a `DILU` preconditioner.

To ensure stability during the simulation, a time-step was chosen that guaranteed both a Courant number $Co < 1$ for the Eulerian phase and $Co^{DEM} < 1$ for the Lagrangian phase. The transient simulation was performed using the PISO scheme with `nCorrectors` 3, which specifies the number of pressure correction loops. The residuals were found to reach convergence at each time-step without any issues.

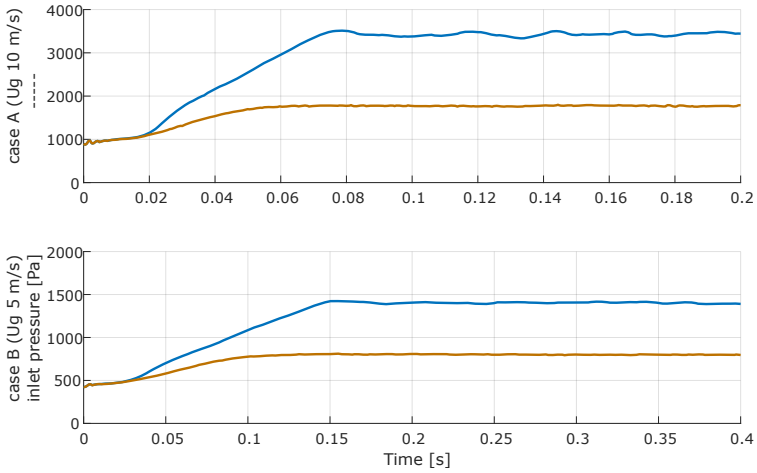

Figure 6. Comparison of the inlet pressure over time for the two methods. Data filtered with moving average over 10^{-3} s (A) and $2 \cdot 10^{-3}$ s (B).

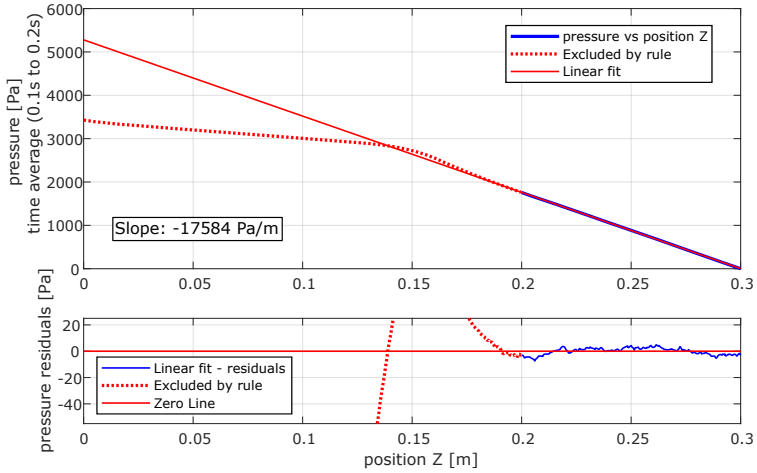

Figure 7. Linear fit of the pressure over the pipe length for CFD-DEM case A, at $U_g = 10$ m/s, and residuals.

3. Results

3.1. **Evaluation of pressure profiles.** To determine whether the simulation had reached the condition of established flow, we evaluated the calculated inlet pressure. As depicted in Fig. 6, the pressure value at the inlet exhibited a distinct oscillation until 0.005 s and 0.010 s respectively for the two velocities considered. The two methods demonstrated almost no difference, and the reason for this can be attributed to the fact that the Eulerian flow was initialized using a different steady-state simulation, and the resulting values were mapped to the E-L case domain. Thereafter, the transient was governed by the rate at which particles filled the pipe. The elbow on the diagram at 0.08 s and 0.15 s, respectively for the two velocities considered and the CFD-DEM case, was clearly linked to the instant at which the particle flow reached the end of the pipe. As a result, these times were utilized to differentiate between transient and established flow conditions.

In addition, it is important to identify the settling length where the flow develops and the remainder of the pipeline where the flow is fully developed in the longitudinal direction. Figure 7 shows the longitudinal pressure of the CFD-DEM case A ($U_g = 10$ m/s), averaged for $t \in [0.1, 0.2]$ s. The pressure demonstrated a nonlinear behavior from the inlet to 0.2 m, representing the development of gas-particle flow. From there to the outlet, the pressure profile becomes linear, indicating a fully developed flow. This was assumed to be the settling length for all other cases.

The inlet pressure profiles over time for the two methods are reported in Fig. 6 and demonstrate substantial differences. The CFD-DEM simulated pressure presents an initial linear increase phase, which is consistent with the pipe filling up with particles after injection. When this phase ends, there is a plateau, indicating stable conditions. The pressure required to transport the material through the pipe, as opposed to gas only, is approximately five times higher, as reported in Tab. 4, indicating that the majority of the energy is required to push the particles through.

MP-PIC underestimates the value, being only around double than the empty pipe simulated condition. This difference between the two methods cannot be ignored and could result in an underestimation of the energy requirement for particle transport through pneumatic conveying. Tab. 4 shows the pressure drop along the pipe at established flow conditions, evaluated through linear fit.

Table 4. Pressure drop along the pipe at the established flow conditions, evaluated through linear fit (example in Fig. 7).

	Slope [Pa/m]	
	Case A	Case B
CFD-DEM	17584	6076
MP-PIC	8639	3293
empty pipe	3164	1465

3.2. **Particle velocity distribution.** In the context of the coupled CFD-DEM model, it has been observed that after the stabilization period, the positions and velocities of particles along the pipe display repeatable behaviors. This section focuses on the velocity distribution of particles along the pipe, which has been analyzed at time $t = 0.19$ s to represent a fully developed flow. Figure 8 summarizes the salient metrics of particle flow for the CFD-DEM case A. A comparison with the MP-PIC case A in Fig. 9 reveals stark differences. As discussed in Section 3.1, there are differences in pressure profiles between the two cases. The velocity diagram also displays distinct behaviors in the two cases. In the CFD-DEM case, particles reach an average velocity of 3.040 m/s, and once the flow is established, the velocity dispersion is relatively low, as evidenced by the error band displaying the standard deviation as $\sigma = 0.61$ m/s. The normalized probability density of the particle location histogram at the top clearly shows that there are volumes with different particle concentrations along the pipe, which move along with the flow. Conversely, the MP-PIC simulation under the same conditions fails to capture the same behavior, as shown in Fig. 9, where the number of particles along the tube is relatively uniform and transitions smoothly, as the particle velocity deviates less significantly from the inlet condition, thereby not displaying the terminal velocity seen in the DEM case.

It is worth reiterating that drag is treated identically in both cases, and the difference in behavior is attributed to the contact and compaction laws, indicating that the CFD-DEM approach provides significantly more information in this case. Figure 10 highlights the difference between the two methods for the inlet velocity of 10 m/s (top graph) and 5 m/s. The average value and dispersion, as the symmetric standard deviation of a normal distribution, are calculated in 100 uniform intervals along the pipe length. The particle velocity for the CFD-DEM simulations tends to a defined dispersion as they progress through the pipe, reaching a stable value that is significantly lower than the inlet velocity after a length of about 0.20 m.

Figure 11 distinctly illustrates a crucial aspect regarding the necessary length to achieve a fully developed flow. The presented diagrams depict the average Y position of particles, binned into 100 segments along the Z direction, for all considered cases. Given the assumptions of laminar flow and uniform velocity injection, the particles tend to travel through the pipe relatively undisturbed in a metastable state. The influence of gravity alters their trajectory, causing them to follow a parabolic path towards the bottom of the pipe, where they subsequently rebound. During this rebound, they initiate disturbances in the incoming parcels, consequently unsettling the metastable equilibrium dictated by the simulation conditions. The flow described in this study attains a developed state, herein referred to as the stable flow condition. Initially, almost no interactions between particles happen, as they differentially accelerate or slow down under the action of drag across the pipe diameter. The action of gravity is important, as it provides the first disturbance to the system. As the gravitational settling takes place, more and more rebounds can take place, resulting in a cascade effect that leads to the stable, pseudo-steady-state behavior previously observed.

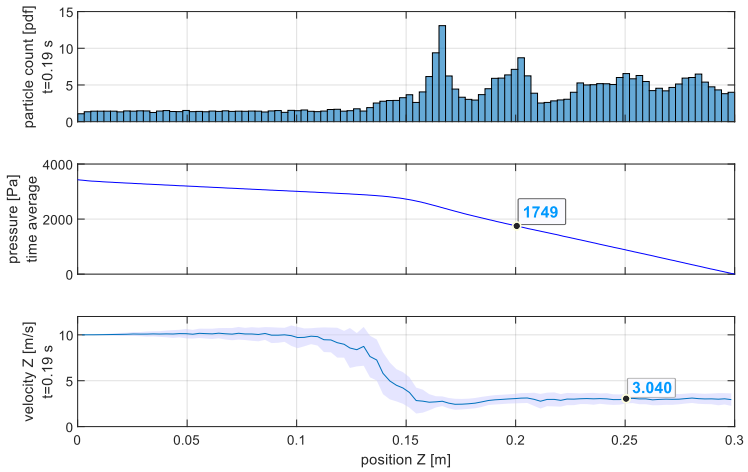

Figure 8. Salient metrics of particle flow in CFD-DEM case A.

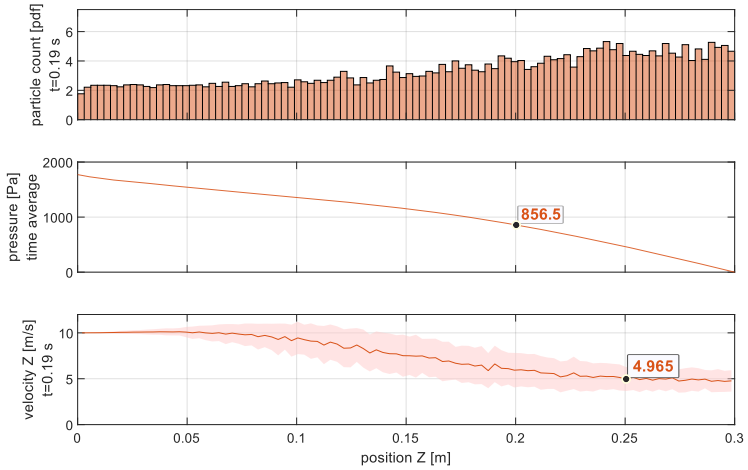

Figure 9. Salient metrics of particle flow in MP-PIC case A.

3.3. **Solids flow rate.** The determination of the solids flow rate is crucial for understanding the material available for deposition and capture over time in Laser Metal Deposition (LMD) processes. In this study, the mass flow rate through the pipe was obtained by counting the mass of each particle escaping the outlet boundary over time. The aim of this study was to investigate the uniformity of this value.

Figure 12 shows the resulting solids mass flow over time for both the CFD-DEM and MP-PIC methods. The data was filtered with a moving average over 10^{-3}s. The 10m/s case is of particular interest and is representative of the 5 m/s case. The graphs have been scaled in both axes to display an equivalent picture. The first parcels arrive at around 0.01 s, which is the time needed to traverse the 0.1 m pipe at the injection velocity of 10 m/s.

The CFD-DEM simulated case shows a noticeable delay between the first particles escaping the boundary and the establishment of the quasi-periodic flow. This is due to the fact that the first few injected particles can traverse the pipe in a diluted phase, without losing much energy. However, as the injection progresses uniformly, the particles progressively slow down due to the impacts. When the flow is established, Fig. 13 displays how the particles in progress form clusters, which move with the flow. These clusters persist until the outlet boundary, giving rise to the solids flow irregularities that this study is interested in.

The deviation from the average mass flow rate is expressed in terms of the Root Mean Square (RMS), a statistical measure that quantifies the spread or variability of a set of values, or a continuous function, around the average. Assuming a finite number n of virtual measurements, the i-th mass flow rate measurement $\dot{m}_i$ and the average at the outlet $\overline{\dot{m}}_{out}$, the RMS value is defined as:

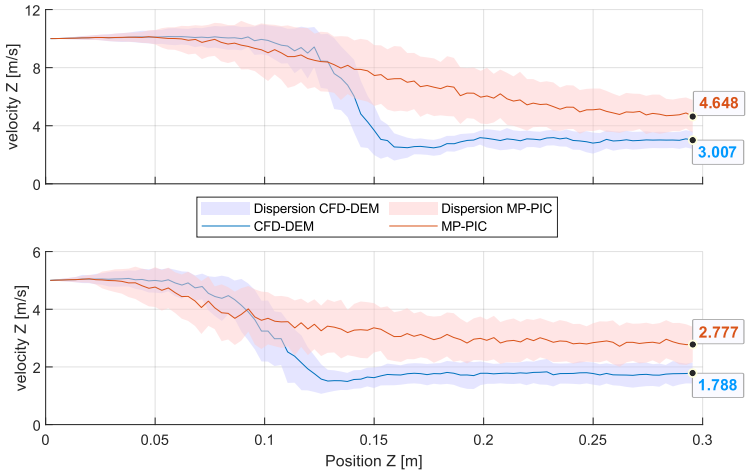

Figure 10. Comparison of the established particle velocity profiles in MP-PIC and CFD-DEM simulations, at $t = 0.2$ s for case A and $t = 0.4$ s for case B.

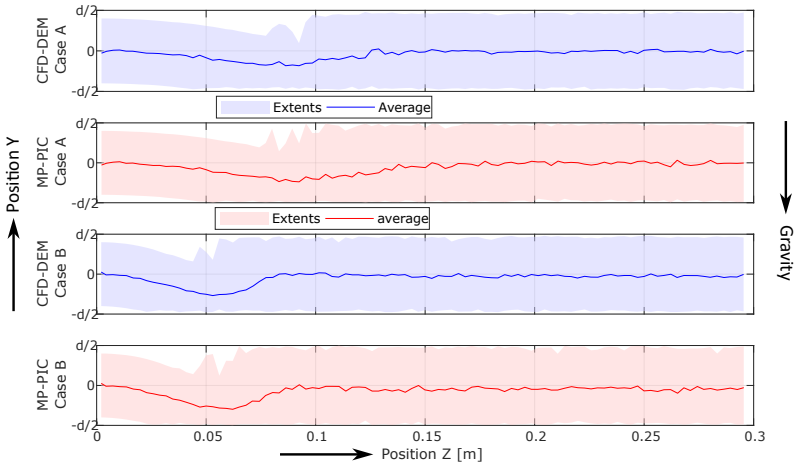

Figure 11. Comparison of parcel position characteristics along the Y-axis, considering the extents (minimum and maximum values) as well as the average positions. The gravitational force acts in the negative direction. The particle positions are depicted at $t = 0.2$ s for Case A and $t = 0.4$ s for Case B, with the positions binned into 100 segments along the Z-axis.

$$\dot{m}_{RMS} = \sqrt{\frac{1}{n}\sum_{i=1}^{n}\left(\dot{m}_i - \overline{\dot{m}}_{out}\right)^2} \tag{5}$$

The MP-PIC method displays a smooth increase to the average value, with low fluctuation after that. On the other hand, the CFD-DEM method shows significant fluctuation in the solids flow rate due to the clusters formed by the particles. The results are presented in Tab. 5, where the average and RMS of the solids flow rates are evaluated at the pseudo steady-state conditions: from 0.1 s and 0.2 s for cases A and B respectively.

3.4. **Computation time.** Table 6 reports the execution times of the presented simulations. It is easy to see that the execution time of the CFD-DEM simulation is three to five times higher than MP-PIC, is dominated by the solution of the Lagrangian domain, and shows a dependency to the number of move-collide subcycles per timestep.

Table 5. Solids flow rates values in g/s.

Case	CFD-DEM			MP-PIC		
	avg	RMS		avg	RMS	
A : 10 m/s	0.3026	0.0829	(27.4%)	0.3075	0.0145	(4.71%)
B : 5 m/s	0.1541	0.0244	(15.8%)	0.1542	0.0078	(5.03%)

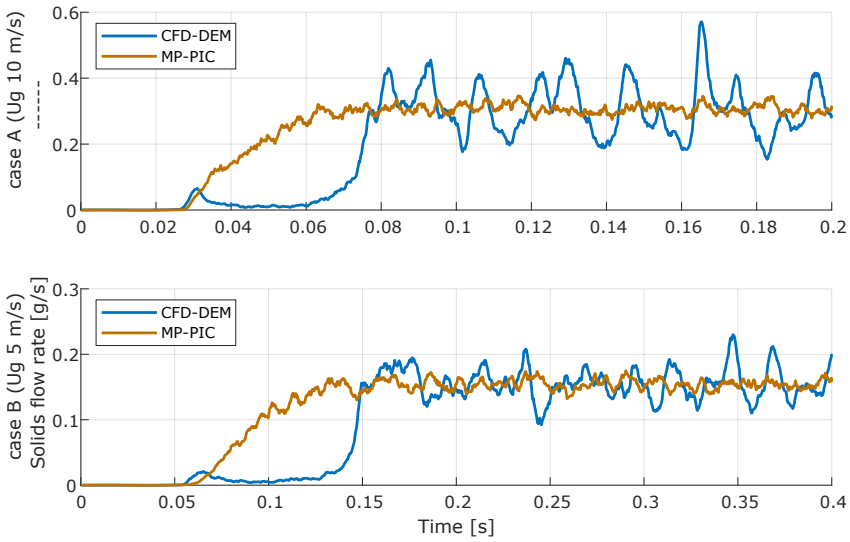

Figure 12. Comparison of the solids flow rate over time for the two methods. Data filtered with moving average over $2 \cdot 10^{-3}$ s (A) and $4 \cdot 10^{-3}$ s (B).

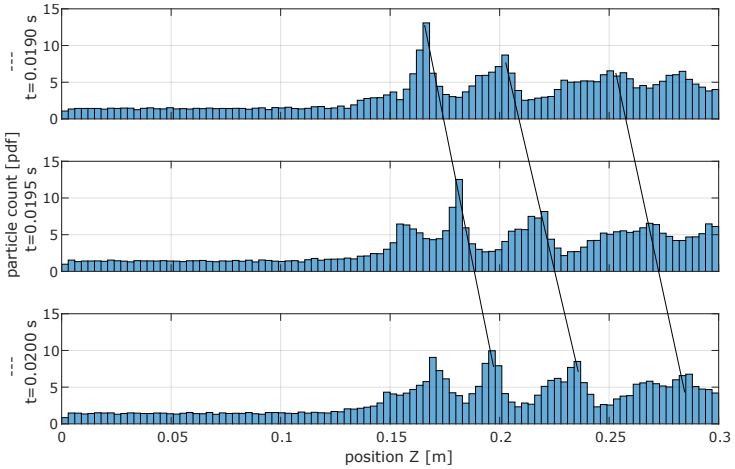

Figure 13. Particle distribution along the pipe, three snapshots at different times for the CFD-DEM case A (10 m/s).

With such a difference, MP-PIC remains an attractive alternative to simulate the pneumatic conveying of fine particles. The presented case, however, shows a limit in its applicability, as it fails to capture the very phenomenon under investigation: the variability of powder mass flow rate over time.

4. Conclusion

In this study, the flow irregularities in a short section of a metal powder feedstock delivery pipeline for Laser Metal Deposition (LMD) were analyzed using two simulation methods available in OpenFOAM v9: MP-PIC and CFD-DEM. The objective was to compare their ability to display periodic phenomena that might appear in the feedstock delivery pipeline. The CFD-DEM method was expected to be more

Table 6. Computation time of the presented cases, on a 4-core PC with an i5-4570 CPU.

	Case A	**Case B**
timestep	$5 \cdot 10^{-6}$ s	10^{-5} s
CFD-DEM		
Execution time	170777 s	258370 s
Avg. number of parcels	16656	16650
Avg. move-collide subcycles per timestep	83	144
MP-PIC		
Execution time	51704 s	45082 s
Avg. number of parcels	11171	11574
Empty pipe		
Execution time (`simpleFoam`)	13.16 s	13.72 s

accurate in representing the physical reality as it directly solves the contact physics, while MP-PIC was less computationally intensive. The benchmark was carried out on the exact same domain, representative of the last section of pipe at the end of the nozzle, and the simulations were conducted with material parameters relative to a sample of powder used in LMD process.

The 4-way coupled, unresolved CFD-DEM simulation displayed a transient time to reach a quasi-periodic transport and a stabilization length, which have been used to determine a quasi-periodic condition in the flow. Careful injection conditions of the parcels result in a meta-stable flow condition. The effect of gravity as the main source of disturbance is highlighted, which drives the sistem to a stable, pseudo-steady-state condition. Self-excited oscillations can be observed in the solids flow rate exiting the conduct, with a noticeable amplitude that is compatible with a contribution to surface irregularities in the LMD process. Waves of solids concentration can be observed along the pipe, developing as soon as the powder starts interacting with the walls. No waves can be observed with MP-PIC simulations. At quasi-periodic conditions, the pressure needed to transport the metal powder simulated using CFD-DEM is around 4 times higher than the sole gas flow, while it is similar to the latter when simulating using MP-PIC. The particle exit velocity is lower than the injection and the continuous phase, and it reaches a quasi-periodic transport velocity which is maintained for the rest of the conveying length. MP-PIC parcels do not display a significant change in velocity compared to injection.

The 4-way coupled, unresolved CFD-DEM simulation revealed a transitional phase before achieving a quasi-periodic transport and stabilization length. Notably, precise injection conditions of the parcels were found to induce a metastable flow state. The influence of gravity as the primary source of disturbance was emphasized, ultimately leading the system to a stable, pseudo-steady-state condition. Interestingly, self-excited oscillations were observed in the solids flow rate exiting the conduit, featuring a discernible amplitude that can be a source of irregularities in processes that employ similar conveying systems, such as LMD. Waves of solids concentration emerged along the pipe, in contrast such waves were absent in MP-PIC simulations. Under quasi-periodic conditions, the pressure required to transport the simulated metal powder using CFD-DEM was approximately five times higher than that of the gas flow alone. Conversely, when simulating with MP-PIC the conveying pressure was underestimated at around double that of the gas flow. The particle exit velocity remained lower than that of both the injection and the continuous phase, achieving a quasi-periodic transport velocity sustained throughout the conveying length. Notably, MP-PIC parcels exhibited a significant smaller change in velocity. These insights provide valuable perspectives on the dynamic behavior of the system and have significant implications for optimizing particle transport in similar contexts.

Given that unresolved CFD-DEM is expected to be more accurate in representing the physical reality, it is recommended that this method be used for future studies on solids flow rate in pneumatic conveying systems, even at the cost of much longer computation times. MP-PIC is a tempting alternative to be used as a fast and efficient method for preliminary studies and design optimization, but the user must consider its limitations. Overall, a better understanding of solids flow rate in pneumatic conveying systems can lead to improved system design and efficiency [3, 17].

Future work could involve studying the effect of different particle properties, such as shape, size, density, and cohesion, on the solids flow rate in pneumatic conveying systems using the CFD-DEM method. The influence of varying gas flow rates, particle injection rates, and pipe geometries on the solids flow rate could also be explored. In addition, it would be interesting to investigate the impact of particle clustering on

the deposition quality of LMD parts, as well as the resulting surface roughness and mechanical properties. Ultimately, a better understanding of these phenomena could lead to improved LMD process control, and the development of more efficient and effective additive manufacturing techniques.

Acknowledgements

This project has received funding from the European Union's Horizon 2020 research and innovation programme under the Marie Skłodowska-Curie grant agreement No. 847624. In addition, a number of institutions back and co-finance this project.

Author Contributions: Conceptualisation, L.P.; methodology, L.P.; software, L.P.; validation, L.P.; formal analysis, L.P.; investigation, L.P.; resources, A.L. and B.A. and I.M.-A.; data curation, L.P.; writing—original draft preparation, L.P.; writing—review and editing, L.P.; visualisation, L.P.; supervision, A.L. and B.A. and I.M.-A.; project administration, A.L. and B. A. and I.M.-A.; funding acquisition, A.L. and B.A. and I.M.-A. All authors have read and agreed to the published version of the manuscript.

References

[1] S. Dadbakhsh, L. Hao, and C. Kong, "Surface finish improvement of LMD samples using laser polishing," *Virtual and Physical Prototyping*, vol. 5, pp. 215–221, Dec. 2010.

[2] F. S. Freeman, B. Thomas, L. Chechik, and I. Todd, "Multi-faceted monitoring of powder flow rate variability in directed energy deposition," *Additive Manufacturing Letters*, vol. 2, p. 100024, Apr. 2022.

[3] A. Singh, S. Kapil, and M. Das, "A comprehensive review of the methods and mechanisms for powder feedstock handling in directed energy deposition," *Additive Manufacturing*, vol. 35, p. 101388, Oct. 2020. [Online]. Available: https://www.sciencedirect.com/science/article/pii/S2214860420307600

[4] M. Murer, V. Furlan, G. Formica, S. Morganti, B. Previtali, and F. Auricchio, "Numerical simulation of particles flow in laser metal deposition technology comparing eulerian-eulerian and lagrangian-eulerian approaches," *Journal of Manufacturing Processes*, vol. 68, pp. 186–197, Aug. 2021. [Online]. Available: https://www.sciencedirect.com/science/article/pii/S1526612521003571

[5] S. Zekovic, R. Dwivedi, and R. Kovacevic, "Numerical simulation and experimental investigation of gas–powder flow from radially symmetrical nozzles in laser-based direct metal deposition," *International Journal of Machine Tools and Manufacture*, vol. 47, no. 1, pp. 112–123, Jan. 2007. [Online]. Available: https://www.sciencedirect.com/science/article/pii/S0890695506000605

[6] M. Mezhericher, T. Brosh, and A. Levy, "Modeling of particle pneumatic conveying using DEM and DPM methods," *Particulate Science and Technology*, vol. 29, no. 2, pp. 197–208, Mar. 2011.

[7] S. Baraldo, A. Roncoroni, F. Palo, and A. Valente, "Multi-physics based methodology for evaluating powder feeding quality for Laser Metal Deposition," *Procedia CIRP*, vol. 107, pp. 623–628, Jan. 2022. [Online]. Available: https://www.sciencedirect.com/science/article/pii/S2212827122003201

[8] K. Higashitani, H. Makino, and S. Matsusaka, *Powder technology handbook*. CRC Press, Taylor & Francis Group, 2020.

[9] A. Levy, *Handbook of conveying and handling of particulate solids*. Amsterdam New York: Elsevier, 2001.

[10] Colin Thornton, *Granular Dynamics, Contact Mechanics and Particle System Simulations : A DEM study*. Springer-Verlag GmbH, Sep. 2015.

[11] G. Klinzing, F. Rizk, R. Marcus, and L. Leung, *Pneumatic Conveying of Solids: A theoretical and practical approach*, 3rd ed. Dordrecht: Springer Netherlands, Jul. 2010. [Online]. Available: https://www.ebook.de/de/product/8905572/g_e_klinzing_f_rizk_r_marcus_l_s_leung_pneumatic_conveying_of_solids_a_theoretical_and_practical_approach.html

[12] D. Mills, *Handbook of pneumatic conveying engineering*. New York: Marcel Dekker, 2004.

[13] F. Zhou, S. Hu, Y. Liu, C. Liu, and T. Xia, "CFD–DEM simulation of the pneumatic conveying of fine particles through a horizontal slit," *Particuology*, vol. 16, pp. 196–205, Oct. 2014. [Online]. Available: https://www.sciencedirect.com/science/article/pii/S1674200114000911

[14] H. Zhao and Y. Zhao, "CFD–DEM simulation of pneumatic conveying in a horizontal channel," *International Journal of Multiphase Flow*, vol. 118, pp. 64–74, Sep. 2019. [Online]. Available: https://www.sciencedirect.com/science/article/pii/S030193221830630X

[15] Y. Alkassar, V. K. Agarwal, N. Behera, M. G. Jones, and R. Pandey, "Transient characteristics of fine powder flows within fluidized dense phase pneumatic conveying systems," *Powder Technology*, vol. 343, pp. 629–643, Feb. 2019.

[16] S. Kuang, M. Zhou, and A. Yu, "CFD-DEM modelling and simulation of pneumatic conveying: A review," *Powder Technology*, vol. 365, pp. 186–207, Apr. 2020. [Online]. Available: https://www.sciencedirect.com/science/article/pii/S003259101930107X

[17] L. Li, Y. Huang, C. Zou, and W. Tao, "Numerical Study on Powder Stream Characteristics of Coaxial Laser Metal Deposition Nozzle," *Crystals*, vol. 11, no. 3, p. 282, Mar. 2021. [Online]. Available: https://www.mdpi.com/2073-4352/11/3/282

[18] M. Sommerfeld, "Analysis of collision effects for turbulent gas–particle flow in a horizontal channel: Part I. Particle transport," *International Journal of Multiphase Flow*, vol. 29, no. 4, pp. 675–699, Apr. 2003. [Online]. Available: https://www.sciencedirect.com/science/article/pii/S0301932203000314

[19] Z. Song, Q. Li, F. Li, Y. Chen, A. Ullah, S. Chen, and W. Wang, "MP-PIC simulation of dilute-phase pneumatic conveying in a horizontal pipe," *Powder Technology*, vol. 410, p. 117894, Sep. 2022. [Online]. Available: https://www.sciencedirect.com/science/article/pii/S0032591022007756

[20] The OpenFOAM Foundation, "Openfoam v9 user guide." [Online]. Available: https://cfd.direct/openfoam/user-guide

[21] D. M. Snider, "An Incompressible Three-Dimensional Multiphase Particle-in-Cell Model for Dense Particle Flows," *Journal of Computational Physics*, vol. 170, no. 2, pp. 523–549, Jul. 2001. [Online]. Available: https://www.sciencedirect.com/science/article/pii/S0021999101967476

[22] F. Li, F. Song, S. Benyahia, W. Wang, and J. Li, "MP-PIC simulation of CFB riser with EMMS-based drag model," *Chemical Engineering Science*, vol. 82, pp. 104–113, Sep. 2012. [Online]. Available: https://www.sciencedirect.com/science/article/pii/S0009250912004502

[23] A. Vaidheeswaran, A. Gel, M. A. Clarke, and W. A. Rogers, "Assessment of model parameters in MFiX particle-in-cell approach," *Advanced Powder Technology*, vol. 32, no. 8, pp. 2962–2977, Aug. 2021. [Online]. Available: https://www.sciencedirect.com/science/article/pii/S0921883121003113

[24] S. B. Kuang, K. Li, R. P. Zou, R. H. Pan, and A. B. Yu, "Application of periodic boundary conditions to CFD-DEM simulation of gas–solid flow in pneumatic conveying," *Chemical Engineering Science*, vol. 93, pp. 214–228, Apr. 2013. [Online]. Available: https://www.sciencedirect.com/science/article/pii/S0009250913000778

[25] C. T. Crowe, J. D. Schwarzkopf, M. Sommerfeld, and Y. Tsuji, *Multiphase Flows with Droplets and Particles*, 2nd ed. Boca Raton, FL: Taylor and Francis Ltd., Aug. 2011. [Online]. Available: https://www.ebook.de/de/product/21177407/clayton_t_crowe_john_d_schwarzkopf_martin_sommerfeld_yutaka_tsuji_multiphase_flows_with_droplets_and_particles.html

[26] J. Kussin and M. Sommerfeld, "Experimental studies on particle behaviour and turbulence modification in horizontal channel flow with different wall roughness," *Experiments in Fluids*, vol. 33, no. 1, pp. 143–159, Jul. 2002.

[27] W. Nan, M. Pasha, T. Bonakdar, A. Lopez, U. Zafar, S. Nadimi, and M. Ghadiri, "Jamming during particle spreading in additive manufacturing," *Powder Technology*, vol. 338, pp. 253–262, Oct. 2018.

[28] Y. Tsuji, T. Tanaka, and T. Ishida, "Lagrangian numerical simulation of plug flow of cohesionless particles in a horizontal pipe," *Powder Technology*, vol. 71, no. 3, pp. 239–250, Sep. 1992.

[29] M. Andrews and P. O'Rourke, "The multiphase particle-in-cell (MP-PIC) method for dense particulate flows," *International Journal of Multiphase Flow*, vol. 22, no. 2, pp. 379–402, Apr. 1996.

[30] S. E. Harris and D. G. Crighton, "Solitons, solitary waves, and voidage disturbances in gas-fluidized beds," *Journal of Fluid Mechanics*, vol. 266, pp. 243–276, May 1994.

[31] S. Song and S. Park, "Unresolved CFD and DEM coupled solver for particle-laden flow and its application to single particle settlement," *Journal of Marine Science and Engineering*, vol. 8, no. 12, p. 983, Dec. 2020. [Online]. Available: https://www.mdpi.com/2077-1312/8/12/983

[32] D. Gidaspow, *Multiphase flow and fluidization : continuum and kinetic theory descriptions*. Boston: Academic Press, 1994.

[33] Z. Yan, S. K. Wilkinson, E. H. Stitt, and M. Marigo, "Discrete element modelling (DEM) input parameters: understanding their impact on model predictions using statistical analysis," *Computational Particle Mechanics*, vol. 2, no. 3, pp. 283–299, Sep. 2015.

[34] K. Washino, E. L. Chan, and T. Tanaka, "DEM with attraction forces using reduced particle stiffness," *Powder Technology*, vol. 325, pp. 202–208, Feb. 2018. [Online]. Available: https://www.sciencedirect.com/science/article/pii/S0032591017308938